Generation and motion control of optical multi-vortex

Xuetao Gan (甘雪涛), Jianlin Zhao (赵建林)*, Sheng Liu (刘 圣), and Liang Fang (方 亮)

Institute of Optical Information Science and Technology, Shaanxi Key Laboratory of Optical Information Technology, School of Science, Northwestern Polytechnical University, Xi'an 710072, China

**E-mail: jlzhao@nwpu.edu.cn*

Received July 17, 2009

The generation and propagation dynamics of multiple optical vortices hosted in a Gaussian beam are experimentally demonstrated by use of the computer-generated holography. Fluid-like motions of the multi-vortex beam are observed owing to the helical phase structure. The multi-vortex beam with identical topological charge presents rotation, which can be suppressed by changing the sign of the topological charge alternately. In addition, the transverse motion control of the multi-vortex is proved by inserting an additional vortex. Finally, rotary and stationary vortex lattices with different periodic arrays are experimentally constructed. The results exhibit potential applications in inducing twisted or stable waveguide arrays and new types of optical traps.

OCIS codes: 050.4865, 090.1760, 260.6042.

doi: 10.3788/COL20090712.1142.

Optical vortices (OVs) are associated with phase singularities (or phase dislocations)[1] carried by different background beams such as Gaussian beams[2]. At the central singular point, OVs hold an undetermined phase and a vanishing amplitude owing to the destructive interference. The phase front of an OV is helical, and the phase gradient on any loop around the central singularity equals $2m\pi$, where m is a signed integer called the topological charge (TC). The sign of TC indicates right- or left-handed helical wavefront. OVs have become an active research topic owning to their intriguing TCs and angular momenta, showing a variety of applications in micro-manipulation[3], quantum communication[4], and digital holography[5]. Moreover, the propagation dynamics of OVs have been intensively investigated in linear and nonlinear optics[6−8], and exhibit many engaging futures. Fluid-like effective interactions between OVs are observed, e.g., conservation of the total charges, rotations (annihilations) of vortex pairs with identical (opposite) charges[6,7]. On the other hand, vortices in other fluid dynamics are generally in the form of a periodic lattice[9,10]. Therefore, generating their counterpart in optics, i.e., OV lattices, is more necessary and can enrich the applications of OVs[11]. OV lattices can be generated from the interference of several plane or sphere beams[12]. However, the formed structures are simple and cannot be readily adjusted. Guo *et al.* promoted a method involving helical phase spatial filtering, which can generate OVs with arbitrary shapes and arrays[13]. In this letter, we adopt another method, i.e., the computer-generated holography[14,15], to generate multiple vortices hosted in a Gaussian beam. Significantly, the fluid-like propagation dynamics of the multi-vortex beams are demonstrated and the possibility to control the transverse motion is proved. Finally, we form vortex lattices with different periodic structures experimentally.

In general, the scalar wave equation for a uniform isotropic medium admits cylindrical wave solutions containing a separable phase term of $\exp(\mathrm{i}m\theta)$, which can describe the screw phase profile of a single-vortex beam, where θ is the azimuthal coordinate. Multi-vortex beams can be constructed in many forms[6,16], but the multi-vortex beams involved in this letter possess phase structures expressed as $\prod_k \exp(\mathrm{i}m_k\theta_k)$[6], where m_k is the TC of the kth vortex, and θ_k is defined as $\theta_k = \arctan[(y-y_k)/(x-x_k)]$, where (x_k, y_k) is the location of the kth phase singularity in the transverse plane. By numerically computing the interferogram between an infinite background field bearing the phase structures mentioned above and a planar reference wave[14], we can obtain the computer-generated holograms (CGHs) used to generate OVs. The wave vector of the planar wave has an angle with respect to the optical axis, which determines the period of the interferogram. To generate the multi-vortex beams, the CGH should contain multiple phase singularities. Typical CGHs for the generation of a single-vortex beam and a multi-vortex beam can be seen in Figs. 1(a) and 2(a1), respectively. They are characterized by forking patterns, which can be used to monitor the position and the TC of phase singularities. Here, we set the TC of an OV, whose forking pattern in the interferogram orientates upward, to be +1 (and *vice versa*).

The experimental arrangement for our illustration of the generation and propagation of multi-vortex beams is similar to that used in Ref. [6]. A 30-mW He-Ne laser beam ($\lambda = 0.63$ μm) is divided by a beam splitter (BS) into two ones. One beam is expanded and used as the reference beam. The other one, whose size can be adjusted by a reversed telescope to different suitable values, is directed onto a spatial light modulator (SLM). The SLM is an amplitude-modulated liquid crystal display (LCD, CRL XGA4) with 1024 × 768 pixels in gray scale (each pixel dimension is 32 × 25 μm^2). It is controlled by a computer and displays the CGHs, whose grating periods are 123 μm. Then, the first order diffracted beam is spatially filtered by a $4f$ system consisting of two 20-cm focal length lens and a pinhole. Finally, the intensity profiles or the interferograms of the phase profiles of OVs, which can be switched by a shutter located in the reference beam, are monitored by a

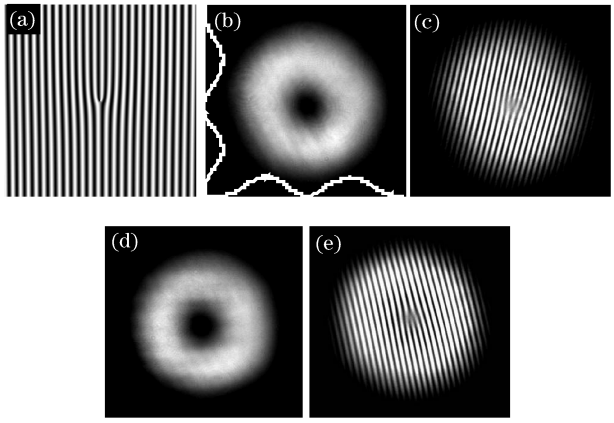

Fig. 1. (a) CGH bearing a single-vortex of unit charge; (b) and (d) are intensity profiles in the +1st and −1st order diffracted beams, respectively; (c) and (e) are interferograms corresponding to (b) and (d), respectively.

charge-coupled device (CCD) camera. Figure 1 gives the generation results of a single unit-charged OV, which is reconstructed by a Gaussian beam with the diameter of 2 mm. Similar doughnut-like intensity profiles are obtained in the +1st (see Fig. 1(b)) and −1st order (see Fig. 1(d)) diffracted beams. However, the corresponding forking patterns in Figs. 1(c) and (e), which have opposite directions, indicate that the TCs of the vortex are $m = 1$ and -1, respectively. In other words, OVs reconstructed in the +1st and −1st order diffracted beams have opposite TCs.

Following the analogy with the interactions between vortex filaments in hydrodynamics, the transverse motions of a vortex pair nested in a common beam were illustrated in Ref. [6]. Here, we demonstrate the rotation dynamics of the multi-vortex beam in free space. First of all, we consider a symmetric square configuration consisting of four phase singularities with charge of $m = 1$. The corresponding CGH and phase structure are presented in Figs. 2(a1) and 2(a2), respectively, and the distance between the adjacent singularities is 1.45 mm. In this experiment, the CGH is illuminated by a Gaussian beam whose diameter has been expanded to 4 mm, and a four-vortex beam can be obtained in the first order diffracted beam. Moreover, the four vortices which we obtain in the +1st (−1st) order diffracted beam all have TC of $m = 1$ (-1). The evolutions of the four-vortex beam can be recorded by translating the CCD camera to different positions along the light path. The propagation distance is regulated as the length between the image plane of the $4f$ system and the position of the CCD. In virtue of a ray optics model, fluid flow about a vortex has been demonstrated[17], i.e., the phase singularity of the vortex will force its background field to rotate around it by the helical phase structure. Additionally, flow velocity is determined by $-\nabla_{\perp}(m\theta)$, which indicates that the flow direction is determined by the TC sign of the singularity. Accordingly, as to the four-vortex beam, the flow of the background field driven by certain singularity can yield the global movement of the other three vortices around it. In other words, the flow established by one singularity will be transported to the other three vortices due to its phase gradient. Figures 2(b1), (c1), and (d1) show the typical experimental intensity profiles at the distances of 5, 15, and 25 cm in the +1st order diffracted path, respectively. From these results, we can find that the four-vortex beam rotates dramatically around its geometry center owning to the joint counterclockwise flow generated by the four phase singularities with $m = 1$. Moreover, the rotation angle at the distance of 25 cm is about 20°. On the other hand, for the vortex flow direction is determined by the sign of TC, the clockwise rotation of the four vortex with $m = -1$ can be observed in the −1st order diffracted beam, as shown in Figs. 2(b3), (c3), and (d3). Under these experimental parameters, we simulate the propagation of a Gaussian beam, which is added by the multi-vortex phase structure in Fig. 2(a2), by employing a modified split-step beam propagation method[18]. The simulation results shown in Figs. 2(b2), (c2), and (d2) are in good agreement with our experimental results. In addition, the interference profiles displayed in Fig. 2(e) verify the phase structures of the four-vortex beam at 25 cm.

In the next step, we insert an additional vortex into the center of the four-vortex configuration and reconstruct five-vortex beams with the same Gaussian beam used in Fig. 2. Correspondingly, another phase singularity should be added into the center of the CGH (Fig.

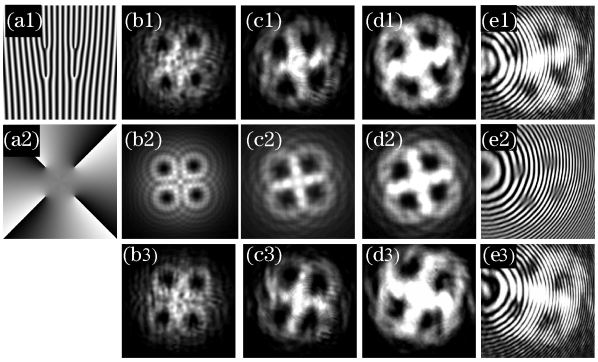

Fig. 2. (a) CGH (upper) and phase structure (lower) of four phase singularities with identical TCs; (b)−(d) intensity profiles of the four-vortex beam at the propagation distances of 5, 15, and 25 cm, respectively; (e) interferograms of (d). The first to the third rows correspond to the experimental and simulation results in the +1st order diffracted beam, and experimental results in the −1st order diffracted beam, respectively.

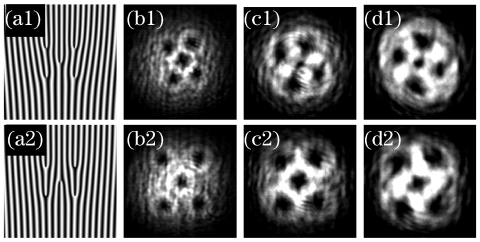

Fig. 3. (a) CGH of five phase singularities; (b)−(d) intensity profiles of the five-vortex beam at propagation distances of 5, 15, and 25 cm, respectively. The upper and lower rows correspond to the central vortex having identical and opposite TC to the other ones, respectively.

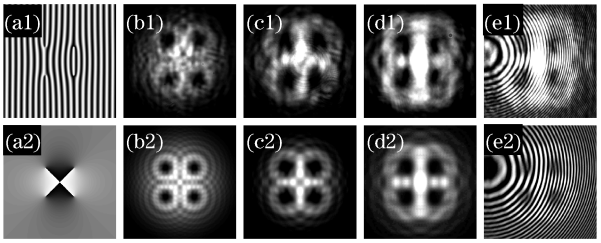

Fig. 4. (a) CGH (upper) and phase structure (lower) of four phase singularities with opposite TCs; (b)−(d) intensity profiles of the four-vortex beam at the propagation distances of 5, 15, and 25 cm, respectively; (e) interferograms of (d). The upper and lower rows correspond to the experimental and simulation results, respectively.

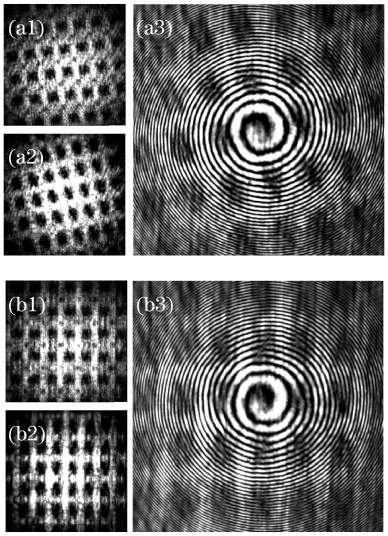

Fig. 5. Square vortex lattice with (a) identical and (b) opposite TCs. (1)−(3) present the intensity profiles at 10 and 20 cm, and the interferogram at 20 cm, respectively.

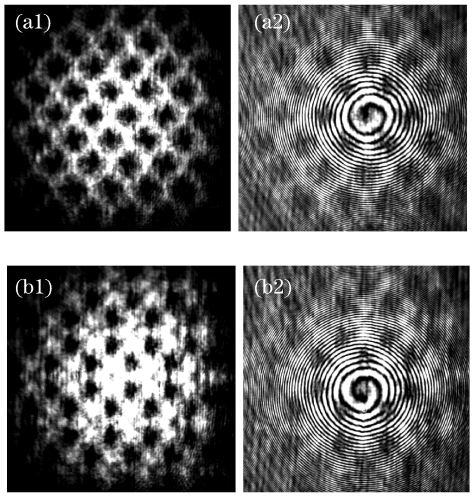

Fig. 6. (a) Rhombus and (b) hexagonal vortex lattices with identical TCs. (1) and (2) display the intensity and interference profiles, respectively.

3(a)). Then, the propagation dynamics of the new five-vortex beam is investigated. Figures 3(b)−3(d) show the evolution results at the distances of 5, 15, and 25 cm, respectively, and the upper and lower rows represent the cases that the TC of the central vortex is equal and opposite to that of the ones, respectively. In the case that five phase singularities all have positive unit charge, the five-vortex beam presents counterclockwise rotation as well, and the relative disposition of the dark cores remains undisturbed. However, compared with the results in Fig. 2, we can find that the rotation rate has been increased, and the rotation angle at the distance of 25 cm is about 30°. This is due to the rotation rate being inversely proportional to the squared distance of the separation between vortices[6]. Remarkably, alternating the TC of the central vortex, we can find that the rotation is suppressed. It can be interpreted by means of the fluid flow of the background field established by vortices. As mentioned above, the center singularity with negative TC will cause the surrounding four vortices hosted in the background field to rotate clockwise as a whole. Accordingly, compared with the rotation of the original four-vortex beam in Fig. 2, the inherent counterclockwise rotation of the surrounding four vortices is retarded by the center singularity. The above results indicate that an additional vortex can accelerate or stabilize the rotation of the multi-vortex beam by changing its TC. This method offers an opportunity to control the fluid-like motions of multi-vortex beams.

To test the suppression on the rotation of the multi-vortex beam by involving phase singularities with opposite TCs, we further generate a four-vortex structure with the CGH and phase structure shown in Figs. 4(a1) and (a2), respectively. It is revealed that each vortex possesses opposite TC to its adjacent ones. Here, the diameter of the input Gaussian beam and the distance between singularities are chosen to be identical with that used in Fig. 2. The propagation dynamics of this four-vortex beam can be concluded from the results in Fig. 4, and the figures represent the same meaning as those in the first and second rows of Fig. 2. The main term responsible for the transverse motion of the multi-vortex is the phase gradient[17]. However, the combination of the vortices with the opposite TCs can eliminate the phase gradient between phase singularities approximately (see Fig. 4(a2)). Thus, as shown in the experimental and numerical results in Fig. 4, no obvious deformation and rotation has taken place. The phase structures of the vortices are proved by the corresponding interference profiles in Fig. 4(e).

Based on the propagation dynamics of multi-vortex beams presented above, we can construct rotary or stationary vortex lattices superimposed on a Gaussian beam. To manifest the vortex lattices markedly, broader input Gaussian beam and smaller distance between singularities should be satisfied. Hence, we adjust the diameter of the input Gaussian beam and the period of the singularities to be 12 and 1 mm, respectively. Figure 5 shows two types of square lattices consisting of phase singularities with unit charge. The vortex lattice in Fig. 5(a) is generated by a CGH containing singularities with identical TC. The intensity profiles at propagation distances of 10 (Fig. 5(a1)) and 20 cm (Fig. 5(a2)) reveal that a rotary lattice is achieved. However, if the phase singularities have the opposite TC sign alternately, they can form

a stationary lattice. As shown in Fig. 5(b), the intensity profiles at propagation distances of 10 (Fig. 5(b1)) and 20 cm (Fig. 5(b2)) have the same configuration without rotation. From the interferogram with a sphere wave in Fig. 5(b3), we can find that the forking pattern at every dark core has opposite direction to the four nearest ones. Hence, by designing suitable CGH containing phase singularities arranged periodically, we can obtain rotary or stationary lattices with different structures and symmetries. Figure 6 gives the experimental results of the rhombus and hexagonal vortex lattices with identical TCs.

In conclusion, we have investigated the generation and motion control of the multi-vortex beams as well as the vortex lattices by designing different CGHs. The phase gradient induced by the helical phase structure can drive the multi-vortex beam with identical TCs to rotate. However, if the multi-vortex beam contains vortices with the opposite TCs, the rotation will be suppressed. Therefore, the transverse motions of the symmetric multi-vortex beams can be controlled by inserting an additional vortex with identical or opposite charge in the geometric center. This appears useful for future all-optical switching and computation, especially in nonlinear optics. Rotary and stationary vortex lattices with different periodic structures are generated experimentally. These vortex lattices can extend the applications of OVs into optical micromanipulation on multi-particle, optically induced twisted and stable photonic lattices[19] and lattice of optical vortex solitons.

This work was supported by the Northwestern Polytechnical University Foundation for Fundamental Research and the Doctorate Foundation of NPU.

References

1. J. F. Nye and M. V. Berry, Proc. R. Soc. Lond. A **336,** 165 (1974).
2. H. Yan, K. Cheng, and B. Lü, Acta Phys. Sin. (in Chinese) **57,** 5542 (2008).
3. M. Gao, C. Gao, and Z. Lin, Chin. Opt. Lett. **5,** 89 (2007).
4. Y.-D. Liu, C. Gao, M. Gao, X. Qi, and H. Weber, Opt. Commun. **281,** 3636 (2008).
5. C.-S. Guo, X. Cheng, X.-Y. Ren, J.-P. Ding, and H.-T. Wang, Opt. Express **12,** 5166 (2004).
6. D. Rozas, Z. S. Sacks, and G. A. Swartzlander, Jr., Phys. Rev. Lett. **79,** 3399 (1997).
7. L. Dong, F. Ye, J. Wang, and Y. Li, Acta Phys. Sin. (in Chinese) **53,** 3353 (2004).
8. X.-T. Gan, P. Zhang, S. Liu, F.-J. Xiao, and J.-L. Zhao, Chin. Phys. Lett. **25,** 3280 (2008).
9. E. J. Yarmchuk, M. J. V. Gordon, and R. E. Packard, Phys. Rev. Lett. **43,** 214 (1979).
10. K. Harada, T. Matsuda, J. Bonevich, M. Igarashi, S. Kondo, G. Pozzi, U. Kawabe, and A. Tonomura, Nature **360,** 51 (1992).
11. K. Ladavac and D. G. Grier, Opt. Express **12,** 1144 (2004).
12. J. Masajada, A. Popiolek-Masajada, and M. Leniec, Opt. Express **15,** 5196 (2007).
13. C.-S. Guo, Y. Zhang, Y.-J. Han, J.-P. Ding, and H.-T. Wang, Opt. Commun. **259,** 449 (2006).
14. Z. S. Sacks, D. Rozas, and G. A. Swartzlander, Jr., J. Opt. Soc. Am. B **15,** 2226 (1998).
15. H. Wang, D. Yang, X. Gan, J. Zhao, X. Ren, and H. Jiang, Acta Opt. Sin. (in Chinese) **29,** 517 (2009).
16. A. G. White, C. P. Smith, N. R. Heckenberg, H. Rubinsztein-Dunlop, R. Mcduff, C. O. Weiss, and C. Tamm, J. Mod. Opt. **38,** 2531 (1991).
17. D. Rozas, C. T. Law, and G. A. Swartzlander, Jr., J. Opt. Soc. Am. B **14,** 3054 (1997).
18. G. M. Muslu and H. A. Erbay, Math. Comp. Sim. **67,** 581 (2005).
19. S. Jia and J. W. Fleischer, Phys. Rev. A **79,** 041804(R) (2009).